Available online at www.sciencedirect.com
ScienceDirect
Catalysis Today 117 (2006) 536–542
CATALYSIS TODAY
www.elsevier.com/locate/cattod

Optimization of a flow reversal reactor for the catalytic combustion of lean methane mixtures

R. Litto [a], R.E. Hayes [a,*], H. Sapoundjiev [b], A. Fuxman [a], F. Forbes [a], B. Liu [a], F. Bertrand [c]

[a] Department of Chemical and Materials Engineering, University of Alberta, Edmonton, Alberta, Canada T6G 2G6
[b] Natural Resources Canada, CANMET Energy Technology Centre Varennes, 1615 Lionel-Boulet Blvd., P.O. Box 4800, Varennes, Quebec, Canada J3X 1S6
[c] Department of Chemical Engineering, Ecole Polytechnique, P.O. Box 6079, Station Centre-Ville, Montreal, Quebec, Canada H3C 3A7

Available online 13 July 2006

Abstract

This paper describes a parametric study of a catalytic flow reversal reactor used for the combustion of lean methane in air mixtures. The effects of cycle time, velocity, reactor diameter, insulation thickness, thermal mass and thermal conductivity of the inert sections are studied using a computer model of the system. The effects on the transient behaviour of the reactor are shown. Emphasis is placed on the effects of geometry from a scale-up perspective. The most stable system is obtained when the thermal mass of the inert sections is highest, while thermal conductivity has only a minor effect on reactor temperature. For a given operation, the stationary state depends on the combination of velocity and switch time. Provided that complete conversion is achieved, highest reactor temperature is achieved with the highest switch time. The role of the insulation is not only to prevent heat loss to the environment, but also to provide additional thermal mass. During operation heat is transfer to and from the insulation. The insulation effect leads to higher reactor temperature up to a maximum thickness. The insulation effect diminishes as the reactor diameter increases, and results in higher temperatures at the centreline.

Keywords: Catalytic combustion; Methane; Reverse flow

1. Introduction

Methane emitted from sources in the oil and gas industry, agriculture, coal mines, etc. is the second most significant greenhouse gas (GHG) after carbon dioxide. Methane has a global warming potential 23 times that of carbon dioxide on a mass basis, therefore the complete combustion of methane will reduce equivalent carbon dioxide emissions by a factor of about 20, even though carbon dioxide is produced. Methane is especially significant in the oil and gas industry; for example, in Canada, methane accounts for 50% of the GHG emissions from the oil and gas business [1]. In the natural gas industry, sources of methane emissions include leaks in gas transmission facilities and in gas production facilities. These emissions also represent wasted energy which, if captured, can be used as a fuel to provide energy for certain applications.

Catalytic combustion is an effective method of burning methane, which offers many advantages over conventional combustion, especially for lean mixtures [2]. The main problem for combustion of lean methane mixtures is the necessity of a high reactor temperature. For ambient temperature feed, some pre-heating would be required to achieve ignition temperature, and to operate the reactor in an auto-thermal mode. To eliminate feed pre-heat, reverse flow operation (RFO) can be used. In a catalytic flow reversal reactor (CFRR) the feed is periodically switched between the two ends of the reactor using control valves. RFO was used quite early for packed beds of solids [3,4] and then extended to catalytic reactors [5]. RFO has been used in many applications [6]. Examples include the oxidation of SO_2 [7–9], methanol synthesis [10,11] and NO_X reduction [12–15]. Although reverse flow operation offers benefits by several routes, one major effect with exothermic reactions is to cause elevated temperatures in the centre of the reactor from the so-called heat trap effect. The process is thus ideal for the catalytic combustion of lean mixtures of hydrocarbons that enter the reactor at standard temperature

* Corresponding author. Tel.: +1 780 492 3571; fax: +1 780 492 2881.
E-mail address: bob.hayes@ualberta.ca (R.E. Hayes).

0920-5861/$ – see front matter
doi:10.1016/j.cattod.2006.06.013

Nomenclature

a_v	surface area per unit volume (m^2/m^3)
C	gas molar density (mol/m^3)
C_P	heat capacity (J/(kg K))
D	dispersion or diffusion coefficient (m^2/s)
h	heat transfer coefficient ($W/(m^2\ K)$)
ΔH^o_R	enthalpy of reaction of methane (J/mol)
k	thermal conductivity (W/(m K))
k_m	mass transfer coefficient (m/s)
k_R	first order rate constant (s^{-1})
r	radial coordinate (m)
$-R_{CH_4}$	rate of disappearance of methane ($mol/(m^3\ s)$)
T	temperature (K)
v_s	superficial velocity (m/s)
Y	gas phase mole fraction
z	axial coordinate (m)

Greek letters

ε	porosity
η	effectiveness factor
ρ	density (kg/m^3)

Superscripts and subscripts

a	axial direction
app	apparent or observed value
eff	effective value in composite medium
f	fluid properties
r	radial direction
S	solid properties

and pressure. In such a case, a quasi-steady state operation may be achieved in which the reactor temperature profile has a maximum value near the centre of the reactor, which slowly oscillates as the feed is switched between the two reactor ends. Because the temperature in the centre of the reactor can greatly exceed the adiabatic temperature rise, energy can be extracted from the centre both as a means of control and as a source of useful energy. For example, in Ref. [16] CFRR was used for catalytic decontamination of waste gases. A heat exchanger was added in the centre of the reactor to remove heat. This ensured that the reactor did not overheat and deactivate the catalyst or damage the reactor. The heat removed from the reactor may be used for tasks such as heating a building or driving a small turbine. The use of RFO for catalytic combustion has been reported [17–22].

Computer modelling can be a valuable tool as an aid in understanding the processes and assisting with design. Models specific to RFO have been reported for a variety of applications, and used to investigate a variety of operating parameters, either from a theoretical view or coupled with experiments. Many models are one-dimensional (1D), and either pseudo-homogeneous or heterogeneous [18,22–31]. Two-dimensional models have also been developed [32,33].

The CFRR shows promise for combustion of lean ambient temperature feed. The technology has been successfully tested in underground coal mine applications, and its use in the oil and gas sector shows promise. However, outstanding issues to resolve include optimization of reactor design and development of robust control strategies. Also, a major concern is the scale-up or scale-down of these units. In particular, the performance change that can occur as the reactor diameter increases, leading to a diminution of the wall effect, has not been thoroughly explored. Many of the modelling studies performed on CFRR used 1D models, which ignore the wall effects, including the effects of insulation. For large diameter reactors, such as those envisaged for coal mine vent gas operation, this may be a reasonable approximation. However, we are currently interested in the installation of smaller units in natural gas compressor stations, and it is expected that wall effects will be much more important in units of this size (diameter less than 1 m). Therefore, we have expanded our earlier work to examine the effects of various operating parameters on these relatively small reactors.

2. Experimental reactor

A CFRR concept appropriate for relatively large flow rates has been reported [32–36]. This design is illustrated in Fig. 1. The reactor has two parallel sections with an internal diameter of 0.2 m mounted side by side and connected by a U-bend at the bottom. Two three-way valves and associated transfer piping allow for either forward or reverse flow operating modes. The reactor system is made from Hastelloy. The reactor walls are 3.2 mm thick with a density of 7800 kg/m^3, a heat capacity of 460 J/(kg K) and a thermal conductivity of 14.3 W/(m K). The

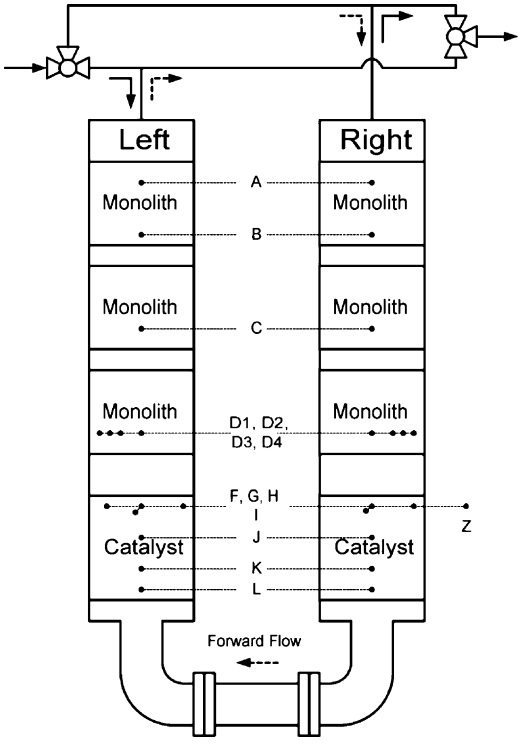

Fig. 1. Reactor schematic showing location of thermocouples and internal sections.

reactor is surrounded by an insulation blanket 0.28 m thick with a density of 128 kg/m^3, a heat capacity of 1340 J/(kg K) and a thermal conductivity of 0.144 W/(m K).

In [35,36] the reactor internals consisted of a combination of open spaces, inert and catalyst sections. The inert sections were ceramic or metal monoliths, or ceramic balls and the catalyst sections were packed beds of Raschig rings with a characteristic length of 7.5 mm and containing a non-noble metal catalyst. Comparison of performance of this reactor for the various inert types is discussed in [35,36]. Hot gas can be extracted at the centre of the U-bend and used as a source of energy. The rate of extraction can be used as a means of controlling the reactor.

3. Computer model

As an aid in design, and to speed up parametric studies, use can be made of computer modelling. Salomons et al. [33] described a two-dimensional heterogeneous continuum model for the CFRR described in Section 2, and validated it using ceramic inert sections under a variety of operating conditions. The model was extended to different insert types and validated by Kushwaha et al. [35,36]. The same model was used in the present investigation, *mutatis mutandis*. For complete details of the algorithm, etc. refer to [33]. The model described in [33] was solved using the finite element method in a Fortran code. For this work, the model was re-written and implemented using COMSOL Multiphysics, and executed using a MATLAB framework. COMSOL uses the Finite Element Method to solve the equations. The COMSOL model was validated using the earlier code [33,34] prior to use. The main equations are presented here for completeness.

Pseudo-steady state mole balance equations were used for both phases. In the packed bed and open sections, mass transfer occurs by dispersion in both axial and radial directions, and by convection in the axial direction. In the monolith sections the structured packing prevents radial dispersion of mass. The generic mole balance for the reactor with a first-order reaction is:

$$\frac{1}{r}\frac{\partial}{\partial r}\left(rD_{\mathrm{r,eff}}C_{\mathrm{f}}\frac{\partial Y_{\mathrm{CH_4,f}}}{\partial r}\right)+\frac{\partial}{\partial z}\left(D_{\mathrm{a,eff}}C_{\mathrm{f}}\frac{\partial Y_{\mathrm{CH_4,f}}}{\partial z}\right) - v_{\mathrm{s}}C_{\mathrm{f}}\frac{\partial Y_{\mathrm{CH_4,f}}}{\partial z}-k_{\mathrm{app}}C_{\mathrm{f}}Y_{\mathrm{CH_4,f}}=0 \quad (1)$$

The apparent reaction rate constant is:

$$\frac{1}{k_{\mathrm{app}}}=\frac{1}{(1-\varepsilon)\eta k_{\mathrm{R}}}\frac{T_{\mathrm{S}}}{T_{\mathrm{f}}}+\frac{1}{k_{\mathrm{m}}a_v} \quad (2)$$

The rate constant k_{R} is evaluated at the surface temperature. For the inert monolith sections, the terms for the radial dispersion and the reaction rate are dropped.

The energy balance for the fluid includes the effects of axial flow, convection, and conduction. The energy accumulation in the fluid is very small compared to the solid and the accumulation term in the fluid phase was dropped. The equation for the fluid phase in the presence of a solid (with or without reaction) is:

$$\frac{1}{r}\frac{\partial}{\partial r}\left(rk_{\mathrm{rf,eff}}\frac{\partial T_{\mathrm{f}}}{\partial r}\right)+\frac{\partial}{\partial z}\left(k_{\mathrm{af,eff}}\frac{\partial T_{\mathrm{f}}}{\partial z}\right) - v_{\mathrm{s}}\rho_{\mathrm{f}}C_{P,\mathrm{f}}\frac{\partial T_{\mathrm{f}}}{\partial z}+ha_v(T_{\mathrm{S}}-T_{\mathrm{f}})=0 \quad (3)$$

For a monolith the radial conduction term is dropped. The energy balance in the solid phase was modelled considering the effects of accumulation, axial conduction, radial conduction, convection, and energy generation by the reaction, as necessary. The form of the equation is the same for both monolith and packed bed sections:

$$\frac{1}{r}\frac{\partial}{\partial r}\left(k_{\mathrm{rs,eff}}r\frac{\partial T_{\mathrm{S}}}{\partial r}\right)+\frac{\partial}{\partial z}\left(k_{\mathrm{as,eff}}\frac{\partial T_{\mathrm{S}}}{\partial z}\right) + ha_v(T_{\mathrm{f}}-T_{\mathrm{S}})+(1-\varepsilon)\Delta H_{\mathrm{R}}\eta(-R_{\mathrm{CH_4}}) = (1-\varepsilon)\rho_{\mathrm{S}}C_{P,\mathrm{S}}\frac{\partial T_{\mathrm{S}}}{\partial t} \quad (4)$$

In the inert monolith sections, the reaction rate term is dropped. Here, $k_{\mathrm{as,eff}}$ and $k_{\mathrm{rs,eff}}$ are the effective axial and radial thermal conductivity of the solid phase, respectively.

For the solid reactor walls and insulation it is necessary to solve the conduction equation in radial geometry. For these two domains the energy balance is:

$$\frac{1}{r}\frac{\partial}{\partial r}\left(k_{\mathrm{S}}r\frac{\partial T_{\mathrm{S}}}{\partial r}\right)+\frac{\partial}{\partial z}\left(k_{\mathrm{S}}\frac{\partial T_{\mathrm{S}}}{\partial z}\right)=\rho_{\mathrm{S}}C_{P,\mathrm{S}}\frac{\partial T_{\mathrm{S}}}{\partial t} \quad (5)$$

The solid thermal conductivity takes on the value for the wall or insulation as appropriate.

4. Results and discussion

A key advantage of a computer model is that it may be used to explore the effects of changing parameters individually. Further, long time experiments can be performed which would be too time consuming or expensive to perform in the pilot or full scale experimental system. This model may also be used to develop control strategies.

In this work the computer model is used to explore the influence of operating parameters, as a precursor step in the development of optimization and control strategies. From our previous experimental and limited modelling work, as well as the literature, a number of variables will be important to the operation. These include the thermal mass and thermal conductivity of the system, the insulation, the fluid velocity, switch time, and reactor geometry. We now present some results and trends based on changing these parameters.

We first define a base case scenario, which is based on the reactor described in [6–9] with the ceramic monolith in the inert sections. The base case superficial velocity at STP was 0.3 m/s and the cycle time was 700 s (switch time 350 s). The methane concentration was 0.6% on a volume basis. Starting from an arbitrary temperature profile, the progression of the centreline axial temperature profile is shown in Fig. 2.

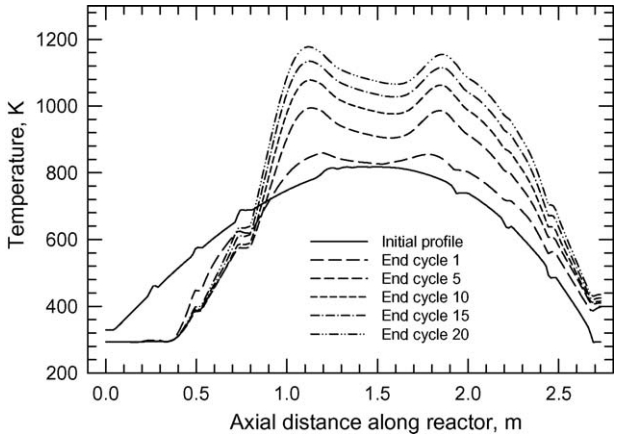

Fig. 2. Development of the centreline axial temperature profile for the base case. The temperature continues to increase with each cycle, and a stationary state is not obtained.

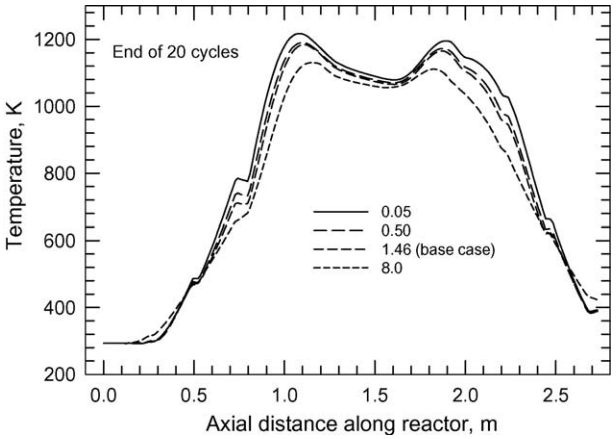

Fig. 4. Centreline axial temperature profile for different thermal conductivities at the end of cycle 20. The effect is relatively minor.

4.1. Effects of thermal properties

In the earlier experimental investigations [35,36] it was seen that the higher thermal mass (product of density and heat capacity) inert sections gave less movement in the axial temperature profiles for a given cycle time. This observation is consistent with intuition; however, in the experimental runs it was not possible to change only a single variable. In the first set of simulations we compare the axial temperature profiles obtained after 20 full cycles with different thermal mass only. We should point out that we have not achieved a stationary state at 20 cycles. Indeed, for these conditions, the stationary state occurs at a temperature higher than the safe operating region for the system. For a series of experiments, the thermal mass was set to a given percentage of the base case. Fig. 3 shows the centreline axial temperature profiles obtained in the middle and at the end of cycle 20. It is clear that the highest temperatures are achieved with the highest thermal mass. This result is in line with expectations. It is evident that for low thermal mass, the outlet temperature of the gas increases, resulting in energy loss from the system, and hence a lower temperature. Further, the movement of the temperature wave during a cycle is the lowest with the highest thermal mass. It is clear that this variable is one of the most important, from a standpoint of reactor stability.

The other principal thermal property is the thermal conductivity of the solid. The key effect of an increase in thermal conductivity is to increase the rate of heat transport through the solid phase. This effect could theoretically be beneficial in smoothing temperature gradients. We had previously noted that metal monoliths gave quite different behaviour to ceramic ones, although as stated out above, this difference could be caused by a number of property changes. It has been pointed out that in the flow direction in a monolith the solid thermal conductivity plays a minor role in axial transport. Fig. 4 shows the result after 20 cycles of changing only the thermal conductivity over a wide range. It appears that the lower thermal conductivity gives a slightly higher centreline temperature, although overall the effect is not that large. The main effect is to promote increased radial conduction, which is the result of heat transfer into the insulation section. These results indicate that the role of the thermal conductivity, within physically attainable bounds, should not be that significant. This is especially important as a contribution to controlling heat transfer effects to and from the insulation.

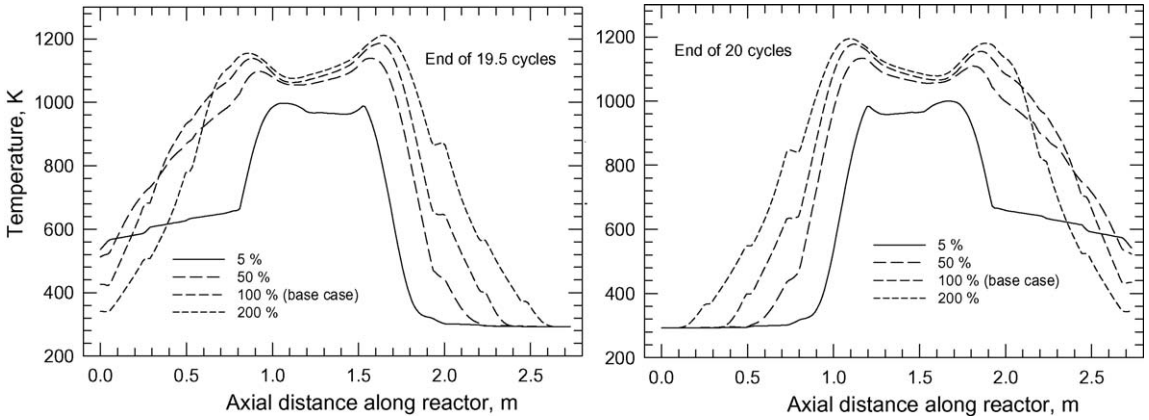

Fig. 3. The centreline axial temperature profile in the middle and at the end of cycle 20 for different thermal mass. The highest temperature and the least movement are seen with the highest thermal mass.

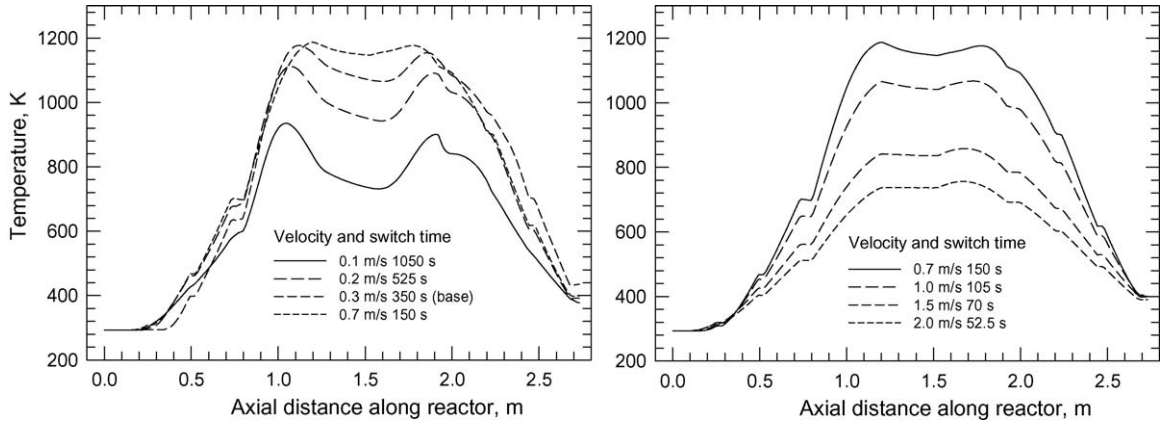

Fig. 5. Centreline temperature profile after 20 cycles for different combinations of velocity and switch time. The product of the two values is a constant.

4.2. Effect of velocity and switch time

The switch time is one of the key variables that can be used to control reactor operation. The best switch time should depend to an extent on the superficial gas velocity, which in turn may be related to the feed concentration. Velocity affects the residence time in the reactor, and hence affects the conversion. The combination of velocity and switch time also determines the movement of the axial temperature profile. The next set of results shows the effects of changing both the velocity and switch time such that the product of velocity and switch time is a constant. Fig. 5 shows the centreline axial temperature profiles after 20 cycles for a wide range of velocity and switch time combinations. When the product of the velocity and switch time is low, the reactor does not achieve the maximum temperature. Indeed, it was observed that for the lowest velocity of 0.1 m/s, the reactor reached a stationary state after five cycles. Increasing the velocity leads to a higher reactor temperature, provided that full conversion of the feed methane is obtained. It was observed that after 0.7 m/s, further velocity increases resulted in incomplete conversion, and as a result the temperature begins to fall.

Changing the switch time alone at a constant velocity will result in more movement of the temperature front in the reactor. The effect is shown in Fig. 6 for a range of cycle times. Longer cycle times lead to higher outlet temperatures, and thus energy loss from the system. Ultimately, longer switch times will lead to extinction of the reaction.

4.3. Geometry effects

Possibly the most important variable from a scale-up standpoint is the effect of geometry. We consider here two geometry effects; insulation thickness and reactor diameter. It has previously been noted [33–36] that the insulation plays a significant role in the reactor operation. The insulation adds thermal mass to the system, and during operation energy is transferred to and from the insulation. Fig. 7 shows the effect of changing reactor diameter using a constant insulation thickness. The axial centreline temperatures after 20 cycles are higher with larger reactor diameter by a significant amount. This result points to a significant wall effect, which is not surprising. With increasing reactor diameter, the radial temperature profiles become flatter, and the insulation effect diminishes, leading to higher centreline temperatures. These results must be included when scale-up is considered. We should point out that based on estimates of gas flowrate from applications in the oil and gas sector, reactor diameters less than

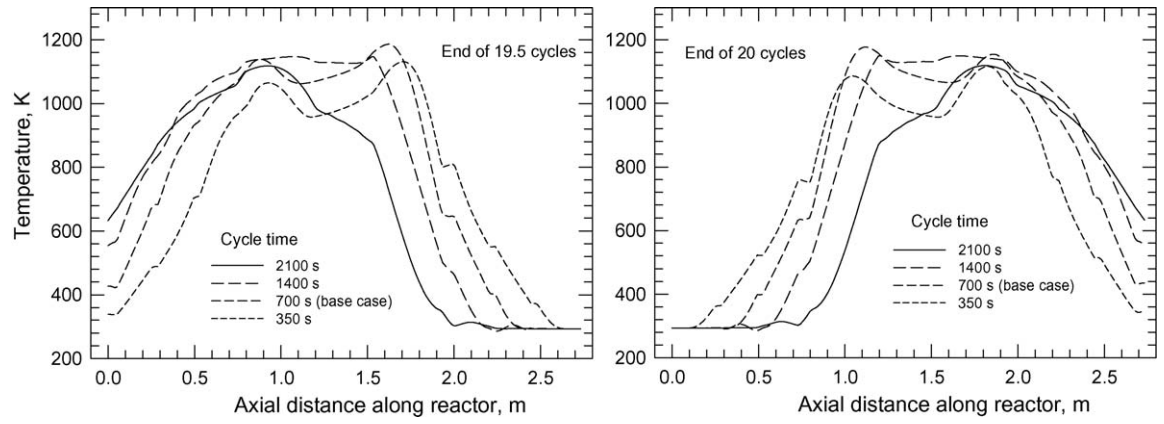

Fig. 6. Centreline temperature profile at the mid-point and end of cycle 20 for different cycle time. The larger cycle time shows more motion of the profile.

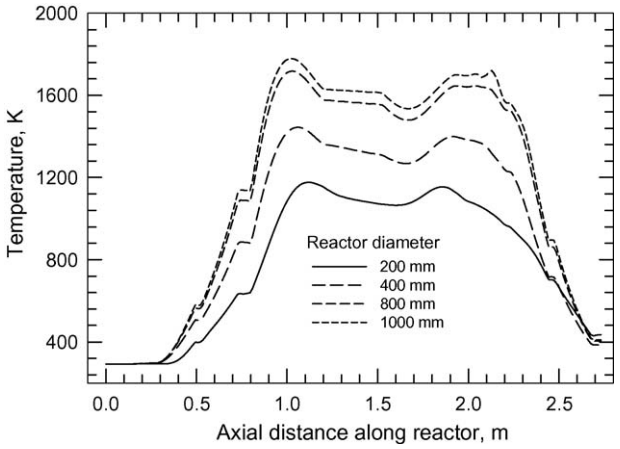

Fig. 7. Axial temperature profiles after 20 cycles at various reactor diameter. The wall effect is evident.

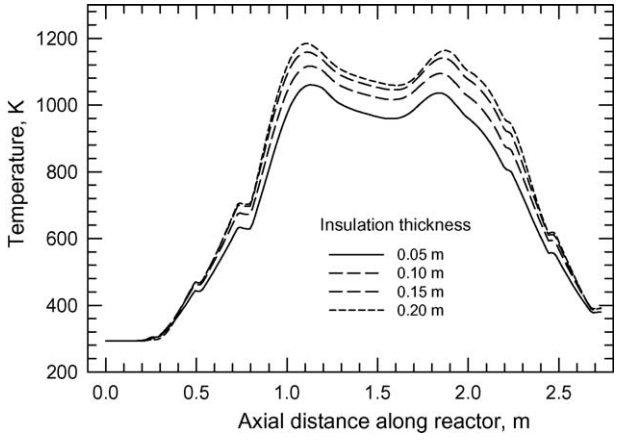

Fig. 8. Axial temperature profiles after 20 cycles at various insulation thickness and constant reactor diameter. Above 20 cm thickness the effect is insignificant.

1 m can be expected, hence attention must be paid to the insulation thermal properties and thickness.

The effect of the insulation can be shown independently by adjusting its thickness from the base case (0.28 m thick). Fig. 8 illustrates the result of increasing the insulation from 5 to 20 cm in thickness with reactor diameter of 200 mm. For a thickness large than 20 cm, no significant difference in the temperature profile was observed using the base case operating conditions. The thickness beyond which no change is observed is related ultimately to the heat transfer rate and the thermal properties of the insulation, which, in terms of a transient heat transfer analysis, are determined by the values of the Biot number and Fourier modulus.

5. Conclusions

It has been observed that systems such as the CFRR demonstrate very dynamic behaviour, with a complex interrelationship among the operating variables. Development of optimization and control strategies must take such relationships into account, and a certain amount of customization towards a particular application is expected. This work is the subject of an on-going investigation. The primary scaling parameter being the reactor diameter, special care must be paid to this variable. For large units, such as those used in coal mine applications, it is expected that the wall effects will be minimal; however, for smaller units in other applications, the two-dimensional behaviour of the reactor cannot be ignored.

Acknowledgements

Financial support for this work was provided by the Natural Sciences and Engineering Research Council of Canada and COURSE (AERI).

References

[1] R.E. Hayes, Chem. Eng. Sci. 59 (2004) 4073.
[2] R.E. Hayes, S.T. Kolaczkowski, Introduction to Catalytic Combustion, Gordon and Breach Science Publishers, Reading, UK, 1997.
[3] F.G.Cottrell, U.S. Patent 2,121,722 (1938).
[4] N. Gilbert, K. Daniels, Ind. Eng. Chem. (1948) 1719.
[5] D.A. Frank-Kamenetski, Diffusion and Heat Exchange in Chemical Kinetics, Princeton University Press, Princeton, NJ, USA, 1955.
[6] Y.S. Matros, G.A. Bunimovich, Catal. Rev.: Sci. Eng. 38 (1996) 1.
[7] G.K. Boreskov, G.A. Bunimovich, Y.S. Matros, A.A. Ivanov, Kinet. Katal. 23 (1982) 402.
[8] Y.S. Matros, Catalytic Processes Under Unsteady State Conditions, Elsevier, Amsterdam, 1989.
[9] G.A. Bunivovich, V.O. Strots, O.V. Goldman, Theory and industrial application of SO_2 oxidation reverse-process for sulfur acid production, in: Y.S. Matros (Ed.), Unsteady State Processes in Catalysis, VPS BV, Ultrecht, 1990.
[10] K.M. Vanden Bussche, S.N. Neophytides, I.A. Zolotarskii, G.F. Froment, Chem. Eng. Sci. 48 (1993) 3335.
[11] S.N. Neophytides, G.F. Froment, Ind. Eng. Chem. Res. 31 (1992) 1583.
[12] Ir.R.P.M. Guit, in: M.P.C. Weijnen, A.A.H. Drinkenburg (Eds.), Precision Process Technology, Kluwer Academic Publishers, Dordrecht, Netherlands, 1993, p. 453.
[13] J.D. Snyder, B. Subramaniam, Chem. Eng. Sci. 53 (1998) 727.
[14] L.N. Bobrova, E.M. Slavinskaya, A.S. Noskov, Y.S. Matros, React. Kinet. Catal. Lett. 37 (1988) 267.
[15] A.S. Noskov, L.M. Bobrova, Y.S. Matros, Catal. Today 17 (1993) 293.
[16] G. Grozev, C.G. Sapundzhiev, Chem. Eng. Technol. 20 (1997) 378.
[17] G.K. Boreskov, Y.S. Matros, in: L.K. Doraiswamy (Ed.), Recent Advances in the Engineering of Chemically Reacting Systems, vol. 142, Wiley, New Delhi, India, 1984.
[18] G. Eigenberger, U. Nieken, Chem. Eng. Sci. 43 (1988) 2109.
[19] Y.S. Matros, A.S. Noskov, V.A. Chumachenko, Chem. Eng. Process. 32 (1993) 89.
[20] C. Sapundzhiev, J. Chaouki, C. Guy, D. Klvana, Chem. Eng. Commun. 125 (1993) 171.
[21] L. van de Beld, R.A. Borman, O.R. Derkx, B.A. van Woezik, K.R. Westerterp, Ind. Eng. Chem. Res. 33 (1994) 2946.
[22] S. Purwano, H. Budman, R.R. Silveston, Y.S. Matros, Chem. Eng. Sci. 49 (1994) 5473.
[23] S.K. Bhatia, Chem. Eng. Sci. 46 (1991) 361.
[24] A. Gawdzik, L. Rakowski, Chem. Eng. Sci. 43 (1988) 3023.
[25] A. Gawdzik, L. Rakowski, Comput. Chem. Eng. 13 (1989) 1165.
[26] V.K. Gupta, S.K. Bhatia, Comput. Chem. Eng. 15 (1991) 229.

[27] T.N. Haynes, C. Georgakis, H.S. Caram, Chem. Eng. Sci. 47 (1992) 2927.
[28] B. Liu, M.D. Checkel, R.E. Hayes, M. Zheng, E.A. Mirosh, Can. J. Chem. Eng. 78 (2000) 557.
[29] B. Liu, M.D. Checkel, R.E. Hayes, Can. J. Chem. Eng. 79 (2001) 491.
[30] B. Liu, R.E. Hayes, M.D. Checkel, M. Zheng, E.A. Mirosh, Chem. Eng. Sci. 56 (2001) 2641.
[31] B. Liu, M.D. Checkel, R.E. Hayes, M. Zheng, E.A. Mirosh, SAE Trans., J. Fuels Lubr. 109 (2001) 15.
[32] F. Aubé, H. Sapoundjiev, Comput. Chem. Eng. 24 (2000) 2623.
[33] S. Salomons, R.E. Hayes, M. Poirier, H. Sapoundjiev, Comput. Chem. Eng. 28 (2004) 1599.
[34] S. Salomons, R.E. Hayes, M. Poirier, H. Sapoundjiev, Catal. Today 83 (2003) 59.
[35] A. Kushwaha, R.E. Hayes, M. Poirier, H. Sapoundjiev, Chem. Eng. Sci. 59 (2004) 4081.
[36] A. Kushwaha, R.E. Hayes, M. Poirier, H. Sapoundjiev, Chem. Eng. Res. Des., Trans. I. Chem. E., Part A. 83 (A2) (2005) 205.